Hindawi
Science and Technology of Nuclear Installations
Volume 2018, Article ID 2914036, 10 pages
https://doi.org/10.1155/2018/2914036

Research Article

Numerical Simulation of a No-Insulation BSCCO Toroidal Magnet Applied in Magnetic Confinement Fusion

Yi Zhang, Yuejin Tang, Ying Xu, Zhong Xia, and Li Ren

State Key Laboratory of Advanced Electromagnetic Engineering and Technology, R&D Center of Applied Superconductivity, Huazhong University of Science and Technology, Wuhan 430074, China

Correspondence should be addressed to Li Ren; renli@mail.hust.edu.cn

Received 11 January 2018; Revised 1 April 2018; Accepted 30 April 2018; Published 31 May 2018

Academic Editor: Arkady Serikov

At present, the Tokamak has become a mainstream form of the magnetic confinement fusion device. The toroidal field (TF) magnet in the Tokamak system is required to generate a high-steady field to confine and shape the high temperature plasma. To secure high current density and high thermal stability, the no-insulation (NI) winding technique is used in the fabrication of the TF magnet. During plasma operation, heat is generated in the TF magnet caused by the interaction with central solenoid (CS) coils, poloidal field (PF) coils, and the plasma current. The heat generated in NI coils is complex owing to the existence of current flow between adjacent turns. Thus, it is necessary to calculate the thermal problems. Taking into consideration the effect of turn-to-turn contact resistance, this paper presents the thermal behavior of a NI toroidal magnet under different operating conditions. The NI toroidal magnet is composed of 10 double-pancake (DP) coils wound with BSCCO tapes. The analysis procedure combines the finite element method (FEM) with an equivalent circuit model. This analysis has applicability and practical directive to the design of cryogenic cooling system for NI toroidal magnet.

1. Introduction

The magnet system is a crucial part of Tokamak machine. It consists of toroidal field (TF) coils, central solenoid (CS) coils, and poloidal field (PF) coils. The magnet system is generally designed to generate a high magnetic field to confine and shape the performance of plasma.

In the process of plasma discharge, one of the essential issues is the operational stability of the magnet system. Generally, the TF coils provide a steady toroidal magnetic field to confine the plasma movement, while CS and PF coils operate in pulse mode to control the plasma current. Thus, during plasma discharge, the TF coils are operating under steady state in a variant magnetic field. The nuclear fusion device contains very strict requirements for the intensity and stability of the toroidal magnetic field. In order to keep the plasma confined and stable, the intensity of the magnetic field requires reaching the Tesla level. For example, the max toroidal magnetic field of ITER system is 11.8 T, as the operation current is 68 kA and the max perpendicular magnetic field on the conductor is approximately 4 T. When a plasma current exists, the current fluctuation of the constant direct current (DC) power supply requires it to be less than 1% to ensure the stability of the magnetic field.

The successful application of superconducting technology to the Tokamak magnet is a major breakthrough in the study of magnetic confinement fusion. With the development in the properties of high temperature superconducting (HTS) conductors, the HTS magnet could be considered as potential Tokamak magnet components with the advantages of higher operation temperature and critical current density [1–3]. At present, the application of HTS in fusion devices mainly focuses on the design and fabrication of high temperature superconducting high current conductor [4–8], the design and fabrication of high temperature superconducting current lead [9, 10], and the concept design and small model fabrication of HTS magnet [11, 12]. It was revealed that when the TF coil system operates at the temperature range of 10 to 20 K, accordingly, the manufacturing and operating cost of the device could be reduced [13]. When the operation temperature is 20 K, the cost of the refrigeration system is about 40 % lower than that under the operating temperature

of 4.5 K, realizing that the conduction cooling technology would be available in the Tokamak magnet system [14, 15]. In general, using high temperature superconducting wire to replace low temperature superconducting wire possesses the following advantages: the higher operating temperature and higher thermal stability, savings in the refrigeration cost, as well as improving the temperature margin. The larger current carrying capacity under high field leads to enhancing the energy density, in addition to decreasing the power consumption. The higher current density can reduce the distance between the center of the magnet and the plasmas, thereby significantly reducing the formation of plasma current. Therefore, the HTS Tokamak system is a significant research direction in the field of nuclear fusion. However, the complex electromagnetic operation environment leads to alternating current (AC) losses induced in TF coils and eddy losses induced in the cooling component of TF coils. Consequently, the temperature distribution of TF coils varies along with time during this procedure, presenting the issues of thermal stability and quench protecting of superconducting magnet.

Recently, we have developed a toroidal magnet with no-insulation (NI) BSCCO superconductors as a series of TF coil prototypes [16]. The NI technique is a promising option for enhancing the operational safety and stability of DC HTS magnets. In the form of an NI structure, the adjacent turns of the coil contact through the metal layer. On the one hand, the coil is more compact and the overall current density of the magnet is enhanced. On the other hand, the NI contact can improve the cooling effect of the coil and reduce heat accumulation. Moreover, according to a previous study, when a thermal runaway occurs in the NI coil, the azimuthal current in the superconductor layer will turn towards the radial direction, which endues a self-protecting performance and a higher thermal stability for the HTS magnet [17]. These advantages cater to the demand for enhanced toroidal magnetic field stability of Tokamak system.

In a previous study conducted by the authors, the construction details of the magnet and test results in liquid nitrogen at 77 K were reported. Accordingly, the magnetic field stability and self-protecting feature of the NI toroidal magnet was verified. The experimental results also show that using BSCCO tape can achieve a lower turn-to-turn contact resistance. Thus, NI BSCCO magnet appears better electromagnetic stability under external disturbance compared to NI YBCO magnet, which is relevant for the assessment of the NI technology. In the present study, the conduction cooling structure is used and the NI toroidal magnet is cooled by Gifford-McMahon (GM) cryocooler to 14 K. The electromagnetic characteristics and thermal stability of magnets under different flow patterns are also simulated and analyzed. The simulation model utilizes finite element method (FEM), in which equivalent circuit of NI magnet is established. The thermal simulation model contains all the structures related to cooling and support. The cooling process is then simulated and different operation conditions are introduced. Moreover, the results of numerical analysis for thermal behavior of the NI toroidal magnet are presented, including energizing process in different charging rate and operating in a variable external magnetic field. The simulation results have practical directive significance to the design of conduction cooling system of NI toroidal magnet, as well as providing basic data and conceptual technical principles for future design, fabrication, and operation management of NI-HTS magnet for the Tokamak.

Table 1: Main parameters of the toroidal magnet.

Parameters	
Number of pancake coils	10
Tape width	4.5mm
Tape thick	0.36mm
Inner radius of coil	31 mm
Number of turns	100
Length of straight section	40 mm
Conductor per coil	72m
Operating temperature	14 K
Critical current	395 A
Max toroidal field	1.02 T
Total contact resistance	$207\mu\Omega$
Self-inductance	71.8 mH

2. Structure of the Toroidal Field Magnet

Table 1 shows the main parameters of the NI toroidal magnet. The NI toroidal magnet is composed of 10 racetrack double-pancake (DP) coils. The DP coils are manufactured by BSCCO tapes of Sumitomo Electric Ind. Ltd. (Osaka, Japan). The coil frame and support structure are made of 304 stainless steel. The cooling plates are made of copper (OFHC). The thickness of cooling plates and support structure are 1 and 2 mm, respectively. Two polyimide plates with thickness of 1 mm are installed on both sides of the DP coil to ensure the insulation between the DP coil and the cooling plate.

The magnet system is cooled by conduction cooling using 2 cryocoolers. The main magnet is cooled by an AL-325 cooler. There are 2 copper conduction cooling plates with thickness of 15 mm, which are installed at the top and bottom of the toroidal magnet. These are connected to the cold stage of the AL-325 GM cryocooler. There are also 16 copper support bars acting as cooling channels around the magnet. The current leads and cold shield are cooled by KDE-415. The first cold stage of KDE-415 is used to cool the cold shield and the high temperature end of the superconducting section of the current lead. The second cold stage is used to cool the low temperature end of the superconducting section of the current lead. The conduction cooling scheme of the magnet system is shown in Figure 1. The details of the toroidal magnet and each double-pancake coils are illustrated in Figure 2.

3. Analysis Method

3.1. Calculation Procedure. There are two methods to deal with the electromagnetic-thermal coupled field calculation of superconducting magnet: direct coupled-analysis model

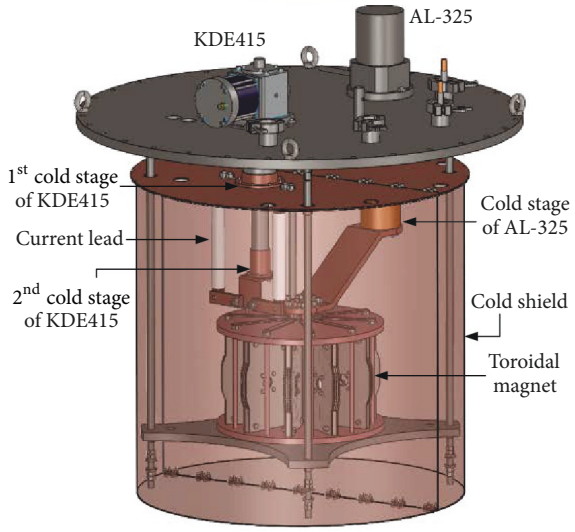

FIGURE 1: The conduction cooling scheme of the magnet system.

and indirect coupled-analysis model. In the indirect coupled-analysis model, time is divided into n substeps. First, starting from the initial value, with calculation of the current and magnetic field after the first substep, heat losses are achieved from hysteresis and eddy current effects. The results are transmitted to the temperature field of thermal analysis for calculating the temperature distribution. Then, the calculation of the next substep is followed. For the direct coupled-analysis model, all the variables (i.e., magnetic field, heat rate, temperature, etc.) must be simultaneously calculated. However, variations in temperature result in changes in the electromagnetic and thermal properties of the material. Thus, cyclic iteration calculation is necessary until the precision of each variable would be within a certain range of error, then the procedure can continue on with the next substep. Otherwise, it is interpreted as nonconvergence. The direct coupled-analysis model is adopted in this study because the electromagnetic and thermal fields of superconducting magnet are tightly coupled, and the material properties of superconductor are very sensitive to temperature.

In the NI magnet, the current contains dual directions in each turn of NI coil because of the no-insulation contact. An equivalent circuit of the NI field coil is required to determine the current distribution. Following, the electromagnetic analysis is used to obtain the AC loss in the magnet, as well as the eddy current loss from the cooling plates and structural supports. The temperature field can be obtained by applying these losses as heat loads into the thermal analysis. Then, a new group of temperature-dependent material properties could be defined in the electromagnetic analysis. The calculation process continues until the result reaches convergence, as displayed in Figure 3.

3.2. Establishment of FEM-Circuit Model. In the present study, the conduction cooling magnet is placed in the Dewar. There are three main heat sources: internal heat caused by the loss generated by the magnet, the heat leakage from supporting structure and current lead, and the heat radiation between the magnet and the cold shield. Since the vacuum pressure in Dewar is 10^{-3} Pa, the heat convection between the magnet and the environment can be ignored. Therefore, the governing equation in the conduction cooling magnet can be presented as a heat conduction differential equation:

$$\frac{\partial T}{\partial t} = \frac{1}{c\rho}\left[\frac{\partial}{\partial x}\left(k_x\frac{\partial T}{\partial x}\right) + \frac{\partial}{\partial y}\left(k_y\frac{\partial T}{\partial y}\right) + \frac{\partial}{\partial z}\left(k_z\frac{\partial T}{\partial z}\right)\right] + \frac{q_v}{c\rho}, \quad (1)$$

where ρ is the density of the materials, c represents the specific heat capacity, T denotes temperature, and q_v is the rate of internal heat generation. x, y, and z are the coordinates in the reference system, and t denotes the time. K_x, K_y, and K_z are the thermal conductivity of the material in the x, y, and z directions, respectively.

Since the BSCCO wire is a multifilament structure, it is composed of superconductor and matrix metal. It is important to handle the electrical and thermal characteristics of the BSCCO HTS coils. However, it is difficult to accurately establish such a complicated model. In the thermal analysis, using effective properties is a useful solution to the problem. The thermal characteristic and volume fractions of the component material are used to obtain the effective thermal conductivity as well as specific heat of the BSCCO wire. The effective thermal conductivity is calculated as

$$k_P = \sum_i f_i k_i \quad (2)$$

$$\frac{1}{k_S} = \sum_i \frac{f_i}{k_i}, \quad (3)$$

where f_i and k_i are the volumetric proportion ($f_i = V_i/V$) and thermal conductivity of the ith material, respectively. k_P is the parallel thermal conductivity and k_S is the series thermal conductivity. The energy change specific heat $\triangle Q$ can be written as

$$\triangle Q = \left(\sum C_i \rho_i V_i\right) \triangle T. \quad (4)$$

The effective specific heat is given by

$$C_{eff} = \frac{\triangle Q}{\rho_{eff} V \triangle T}, \quad (5)$$

where $\triangle T$ is the temperature variation, V represents the volume, and ρ_{eff} denotes the effective density of the HTS tape, which is presented as

$$\rho_{eff} = \sum \rho_i f_i. \quad (6)$$

Owing to the existence of polyimide insulating plate between each single pancakes, a NI double-pancake coil is equivalent to 2 single pancake coils in series. Figure 4

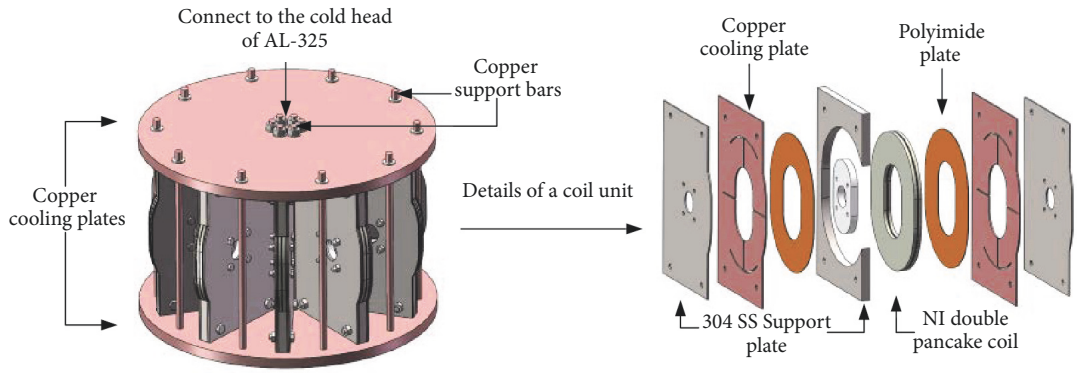

FIGURE 2: Structure details of the NI toroidal magnet and each double-pancake coil.

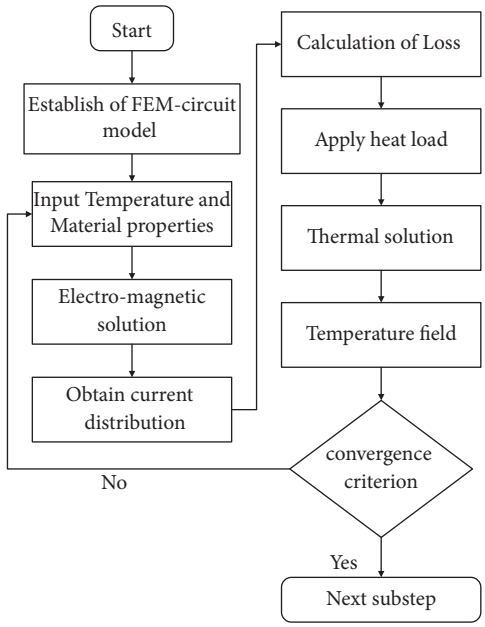

FIGURE 3: Cyclic iteration calculation procedure of the electromagnet-thermal analysis.

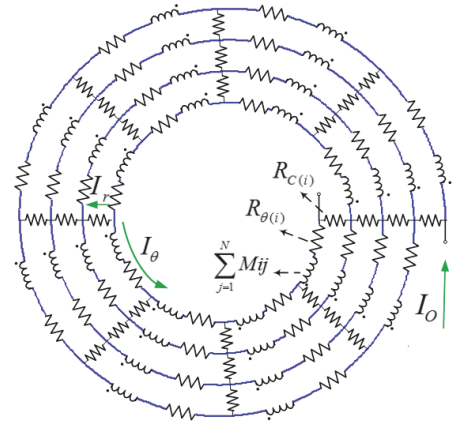

FIGURE 4: Equivalent circuit of a NI single pancake coil.

illustrates the equivalent circuit of NI single pancake coil. The NI coil is divided into N units, where N is the number of turns [18, 19]. Each unit contains an inductance $\sum Mij$ in series with the resistance R_θ. Adjacent turns are connected in parallel with contact resistance, R_c. I_θ and I_r are the currents flowing in the azimuthal and radial directions, respectively. R_θ represents the characteristic resistance of each turn in the azimuthal direction. $\sum Mij$ includes the self and mutual inductances of the inductance units. The inductance $\sum Mij$ can be obtained by the finite element model built by turns: in the finite element model of electromagnetic analysis, the size of the superconducting coil is established by superconducting portion, and the thickness of the superconducting layer is about 1 micron. Each element of per turn of the coil in the FEM model is coupled to the inductors in the circuit model. Thus, the inductance $\sum Mij$ in the circuit can be carried through the FEM model. I_O is the operation current flow through the current lead. $R_{C(i)}$ denotes the i^{th} turn-to-turn contact resistance, which is calculated as follows [20]:

$$R_{C(i)} = \frac{R_{ct}}{(2\pi r_n + 2l)\, w}. \tag{7}$$

In (7), R_{ct} is the turn-to-turn contact resistivity. r_n, l, and w are the radius of the n^{th} turn, straight length of racetrack coil, and width of HTS tape, respectively.

The characteristic resistivity ρ_{sc} is calculated based on Faraday's law and E-J power law, in which it is expressed as

$$\frac{\partial(\mu_r \mu_0 \mathbf{H})}{\partial t} + \rho_{sc} \nabla \times \mathbf{J} = 0, \tag{8}$$

where

$$\mathbf{J} = \nabla \times \mathbf{H},$$
$$\rho_{sc} = \frac{E_0}{J_c(B)} \left| \frac{J}{J_c(B)} \right|^{n-1}. \tag{9}$$

In (8) μ_0, μ_r, and ρ_{sc} are the vacuum magnetic permeability, relative magnetic permeability, and resistivity of the superconductor, respectively. μ_0 and μ_r are $4\pi \times 10^{-7}$ H/m

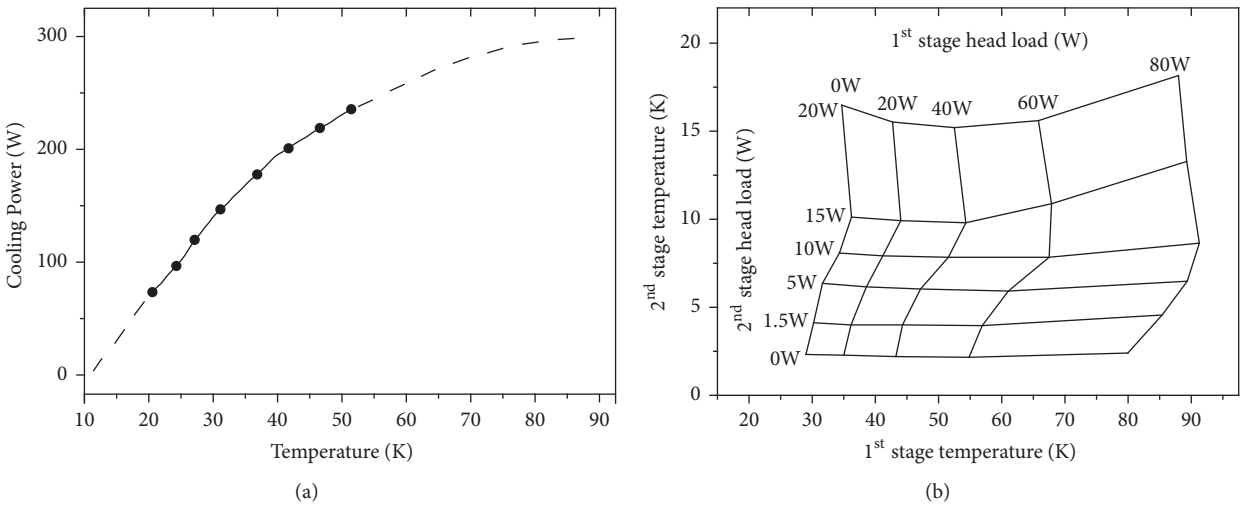

Figure 5: Cooling power along with temperature: (a) AL-325; (b) KDE-415.

and 1. E_0 denotes the electrical field criterion of 1 $\mu V/cm$. The magnetic field dependent critical current density $Jc(B)$ is calculated by [21]

$$J_c(B) = J_{c0} \times \left(0.9756 \times e^{(-5.28\times B\perp)} + 2.05 \times e^{(-0.1106\times B\perp)}\right), \quad (10)$$

where

$$J_{C0} = \alpha \left[1 - \left(\frac{T}{T_C}\right)^2\right]^{1.5}. \quad (11)$$

J_{c0} is the self-field critical current density, T_c denotes the critical temperature of 110 K, and α is the value of the self-field critical current at zero magnetic field. $\alpha = 3.98\times10^8$ A/m^2 is used in the analysis representing $J_{c0} = 0.5\times10^8$ A/m^2 at 14 K [22].

When the magnet is in the excitation process, the magnet loss is composed of two parts: the hysteresis loss P_H of superconducting tapes and the joule loss P_C caused by the contact resistance between adjacent tapes. The resistivity and hysteresis loss of the superconducting layer is calculated by electromagnetic analysis. The operation current I_O is then applied in the transient analysis. From step by step, the azimuthal current and radial current of any time point can be obtained, and the unit of I_r is A. Then the joule loss of the turn-to-turn contact resistance is calculated. According to the critical current density presented by (10) and (11), the hysteresis loss power of the i^{th} inductor element $P_{H(i)}$ is expressed as

$$P_{H(i)} = \int_{\Omega_{(i)}} E \cdot J dv, \quad (12)$$

where $\Omega_{(i)}$ is the volume of the i^{th} superconductor inductor. The joule loss power of each turn-to-turn contact resistance $P_{C(i)}$ is obtained by calculating the contact resistance and radial current:

$$P_{C(i)} = I_{r(i)}^2 \cdot R_{C(i)}. \quad (13)$$

The heat radiation energy between the magnet and the cold shield should also be taken into account in the thermal characteristic analysis. The energy balance formula for thermal radiation is given by Siegal and Howell [23], expressing a relationship between the energy loss and the surface temperature, which can be written as

$$Q_{Ri} = \frac{\sigma\left(T_i^4 - T_j^4\right)}{\left(\left(1-\varepsilon_i\right)/A_i\varepsilon_i + 1/A_iF_{ij} + \left(1-\varepsilon_j\right)/A_j\varepsilon_j\right)}, \quad (14)$$

where ε_i denotes the effective emissivity of surface i, F_{ij} is the radiation view factor, A_i is the area of surface i, Q_{Ri} is the power loss of surface i, σ represents the Stefan–Boltzmann constant, and T_i denotes the absolute temperature of surface i. The radiation boundary is specified on the exterior surfaces of the magnet and the cold shield. The adiabatic boundary is assigned to the rest of the surfaces in the Dewar. In order to reduce the effect of radiation leakage heat on the magnet, heat shield papers are used on the surface of the cold shield and the external surface of the magnet. The effective emissivity is chosen to be equal to 0.1 in the thermal analysis.

In order to define the boundary conditions of the thermal simulation model, heat convection is used on the surface of the cold stage of the cryocooler. The temperature-dependent cryocooler load maps of AL-325 and KDE-415 are depicted in Figure 5 [24, 25]. The temperature at the outside terminal of the current lead is set as 293 K, which is the room temperature.

4. Operating Conditions of the Toroidal Magnet

4.1. Cooling of the Magnet. Figure 6 shows the variations of temperature along with time at the point A (top of the NI

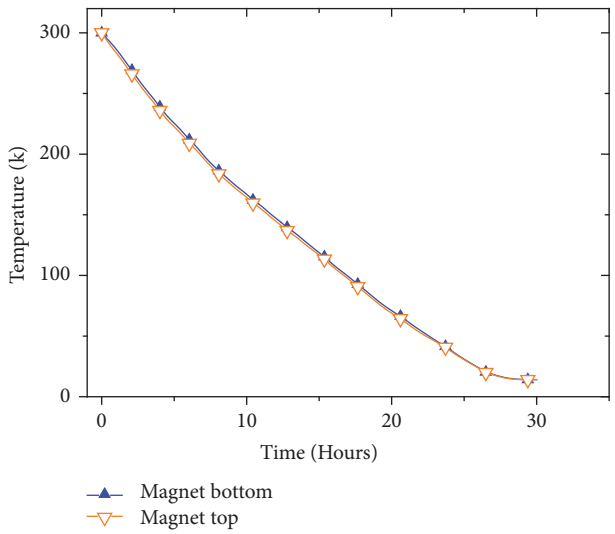

Figure 6: Temperature variation of the magnet in cooling process.

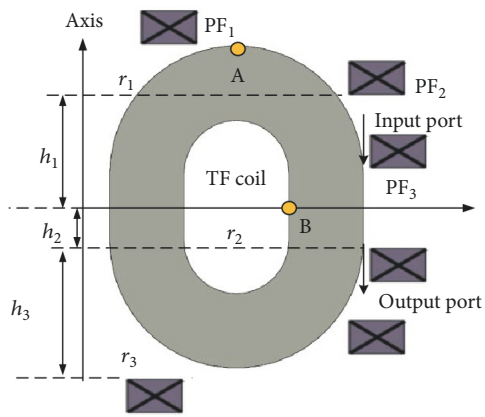

Figure 7: The position of PF coils and TF coil.

DP coil) and point B (middle of the NI DP coil); the position of A and B is shown in Figure 7. The maximum difference of temperature between points A and B is 2 K during the cooling process. This is owing to the absence of insulation layer between adjacent turns. The DPCs have a preferable isotropy of heat conduction in the radial direction. After about 30 hours have passed, the temperature of the entire magnet tends to be stable, where the magnet is cooled to 14 K.

4.2. Operating Current of the Magnet. Generally, there are 6 PF coils in the Tokamak magnet system. The current of each PF coil is a different pulse wave and is controlled by the feedback of plasma current [26]. The operating current of PF coils is simplified in order to conduct an easy analysis. In this study, the current of PF coil is simplified to a triangular wave, which is sufficient for producing a variable magnetic field. The structure of each unit, which consists of one TF coil and six PF coils, is shown in Figure 7. The position of current input port and output port is at the outside of coil. Each PF coil is a double-pancake coil manufactured by BSCCO tape with insulation layer, and the number of turns is 80. The location of PF coils is defined by r_i and h_i. r_1, r_2, and r_3 are 170, 180, and 55 mm, and h_1, h_2, and h_3 are 60, 20, and 90 mm, respectively. In this analysis, two operational conditions are analyzed. In condition A, the TF coils are excited to 395 A and kept steady until the magnetic field saturates from the charging delay. In condition B, the magnetic field of TF coils is saturated under 395 A and kept in a steady state. The PF coils are then excited by triangular current with the current amplitude I_d (from 25 to 125 A) and changing rate K (from 25 A/s to 250 A/s) in one cycle. The operating current waveform in TF coils and PF coils are displayed in Figure 8.

5. Results of Numerical Simulation of Thermal Behavior

The loss in the NI toroidal magnet is composed of the hysteresis loss in superconducting tapes, the turn-to-turn loss from contact resistance, and the eddy current loss in metal component. In this study, the losses and temperature rise in NI coil were assessed during energizing and interaction with PF coils.

5.1. Energizing. According to a previous study performed by the authors, the NI toroidal magnet possesses excellent magnetic field stability benefited from the R_C in the radial direction, characterizing the typical electromagnetic behavior of an RL parallel circuit in time-varying conditions. This advantage caters to the demand for enhanced toroidal magnetic field stability of the Tokamak system. However, this characteristic also brings about a long time constant of charging. Thus, different charging rates are studied to meet the requirement of practical engineering. In condition A, only the TF coils are energized. The transport current is ramped to the rated current of 395 A with the current ramp rates of 0.1, 0.5, 1, 5, and 10 A/s, respectively. The losses and duration of magnetic field saturation (99%) vary with ramping rate, which are displayed in Figure 9. During excitation, when the ramping rates are 10, 5, 1, 0.5, and 0.1 A/s, the turn-to-turn losses are 5557.3, 5354.5, 4079.5, 3069.5, and 957.2 J, and the hysteresis losses are 636.5, 618.3, 378.8, 209.7, and 101.1 J. The turn-to-turn loss is a major part, which is nearly one order of magnitude higher than the hysteresis loss. Meanwhile, the value of eddy current losses is only a small part of total losses, which are 212.9, 207.3, 183.8, 150.4, and 81.6 J. That is owing to the fact that the joule heating between adjacent turns is very large, and the long charging delay causes the magnetic field to slowly vary. When the charging rate increases to certain extent, the excitation loss will significantly increase, and the magnetic field saturation time will decrease. When the ramping rate exceeds 5 A/s, both the magnetic field saturation time and excitation loss reach a stationary value. This can be explained as follows: a redistribution procedure of current exists during the charge of the NI coil. The rate of current flow from turn-to-turn contact to the superconducting layer has a maximum value, which is only related to the coil inductance and contact resistance and is independent of charging rate.

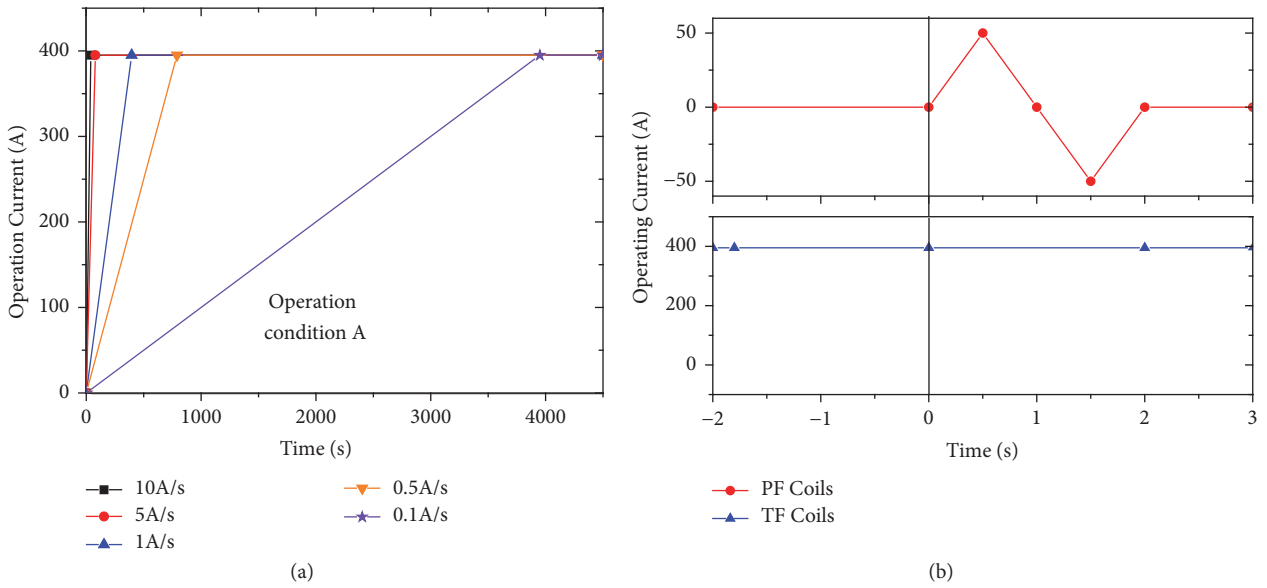

Figure 8: Operating current of PF coils and TF coils: (a) condition A: energizing process of TF coils; (b) condition B: interaction with PF coils.

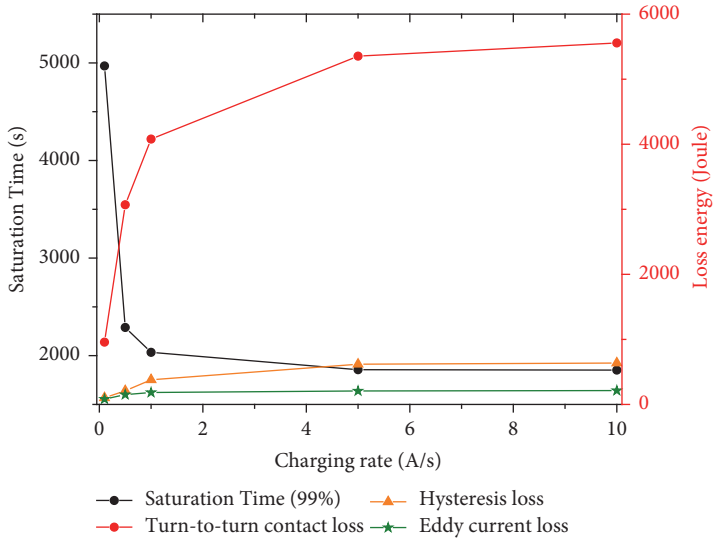

Figure 9: Magnetic field saturation time and losses vary with charging rate.

This specified value limits the magnetic field saturation time of NI coil. As the charging rate increases to 10 A/s, the magnetic field saturation time almost reaches the minimum value (1852 s). Following, the increase of ramping rate does not contribute to the decrease of magnetic field saturation time. The total magnet loss power in different ramping rates along with time is shown in Figure 10. The peak value of loss power increases with ramping rate, and the maximum temperature growths under the rates of 0.1, 0.5, 1, 5, and 10 A/s are 0.02, 0.09, 0.17, 0.56, and 0.93 K, respectively. These results show that an appropriate ramping rate can reduce the charging delay to meet the actual needs, as well as control the increase of temperature within engineering requirement.

5.2. Interaction with PF Coils. In condition B, the thermal behavior of NI TF coil is related to the operating current of PF coils as shown in Figure 8(b). An example of increase of temperature varying with time of the NI TF coil is shown in Figure 11. In earlier period (before 0.6 s), the increase of temperature appears at the top and bottom of the outer layer. This can be explained as follows: the magnetic field of PF coils is mainly perpendicular to the tapes at the top and bottom of the TF coil and parallel to the tape at straight-line segment. The critical current density of superconducting tape is significantly reduced owing to the perpendicular magnetic field. As a result, the AC loss at the top and bottom is much larger than the straight-line portion. After 1.2 s, the

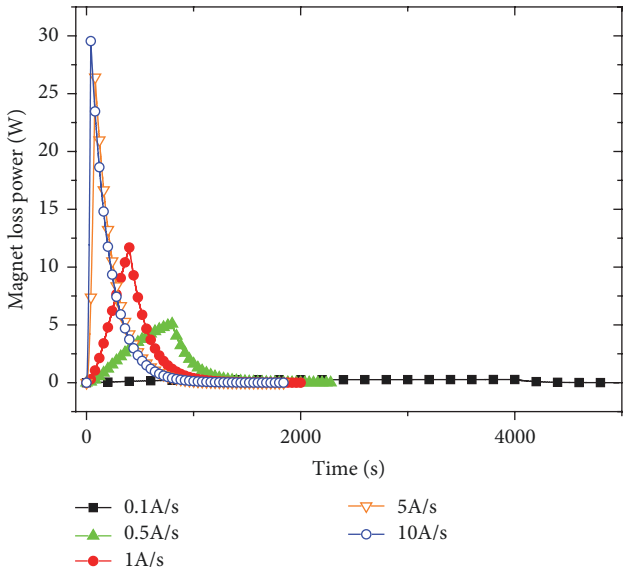

Figure 10: Total thermal loss power of the magnet along with time under different charging rates.

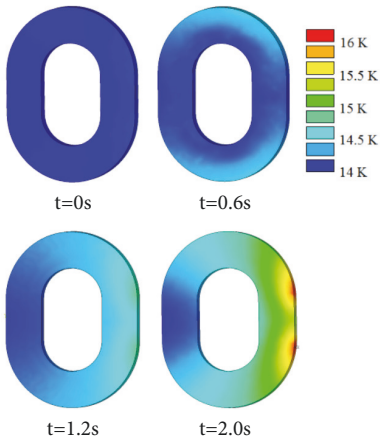

Figure 11: Temperature distribution of TF coil along with time in operational condition B when I_d = 50 A and K =100 A/s.

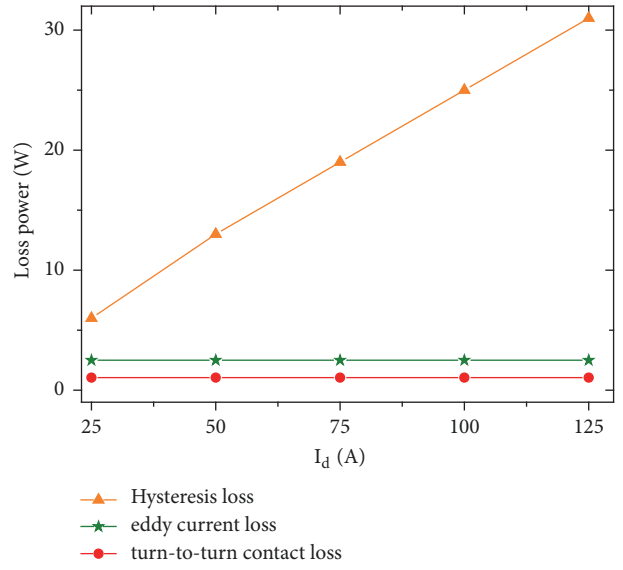

Figure 12: Loss dependence on I_d, with a constant K of 50 A/s.

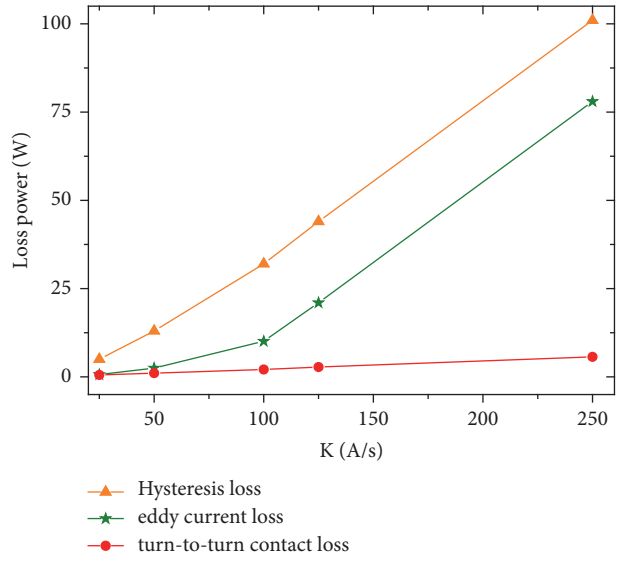

Figure 13: Loss dependence on K, with a constant I_d of 50 A.

temperature near the current input port and output port is remarkably higher than other parts of the TF coil. This is attributable to the fact that the tape at the end of the port is not in thermal contact with the coil; the heat generated in the tape can not be transmitted through metal contact. Thus, the accumulation of heat is more rapid than inside the NI coil, where the heat generation could bypass through the turn-to-turn contact and suppressing temperature rise. The temperature difference between the current port and the NI coil is less than 2.3 K. Moreover, in another position of the NI coil away from the current port, the temperature is much more uniform as the temperature difference at the left part is less than 0.5 K. Thus, the thermal conductivity in the radial direction has been greatly improved compared with the insulated coil, allowing it to become relatively more uniform, contribute to the reduction of temperature difference in the radial direction, and enhance the thermal stability.

In addition, the components of the NI coil losses and their variations with current wave are analyzed. The average loss power dependence on I_d and K is shown in Figures 12 and 13. In the interaction with PF coils, the major loss in NI TF coils is hysteresis loss. This is because the direction of changing magnetic field is parallel to the cooling plate and perpendicular to the axis of NI TF coils, so the induced current in cooling plates and the induced voltage in NI coil are not high. Consequently, the eddy current loss and turn-to-turn contact loss are relatively low. On the other hand, the direction of the changing magnetic field is perpendicular to

some parts of the arc section of NI coil, which may cause a large amount of hysteresis loss. The hysteresis loss shows a linear increasing trend with I_d and K. However, the eddy current loss tends to rapidly increase with the increase of K. Besides, the turn-to-turn loss remains limited, which is entirely different from condition A. The achieved results demonstrate that the faster the ramping rate of PF coils current is, the more losses and higher temperature rises are generated. In order to ensure thermal stability of NI TF magnet, different issues should be taken into account in varied operational conditions.

6. Conclusion

This study aims to describe the analysis procedure considering the influence of PF magnetic field. The numerical simulation results show that (1) when the magnet is charged in different rates, the magnetic field saturation time and excitation loss are different, so it is necessary to choose an appropriate charging rate to meet the engineering requirements and control the heat load; (2) when the magnetic field of PF coils affects the TF coils, the components of the thermal losses of the magnet are different from traditional insulating magnets. The temperature distribution in the DPC is relatively uniform because of the turn-to-turn metal contact. Moreover, there are dangerous areas with higher temperature rise near the current port, which still require further optimization of the electromagnetic design and strengthening of the capacity of conduction cooling to avoid quench. The simulation result can be used to predict the losses and temperature distribution along with time variation and could assist scholars in understanding how to improve the design of the cooling system of NI toroidal magnet made of a single tape. However, the behavior of huge magnet wound of conductors made of a large number of superconducting tapes may be different from a TF magnet made of a single tape. Thus, long-term research and development program is still needed to demonstrate the feasibility of HTS NI TF magnets.

Data Availability

The data used to support the findings of this study are available from the corresponding author upon request.

Conflicts of Interest

The authors declare that there are no conflicts of interest regarding the publication of this paper.

Acknowledgments

This work was supported in part by the National Natural Science Foundation of China under Grant 51677080 and in part by the Science and Technology Project of Hubei Electric Power Company (SGCC) under Grant SGTYHT/16-JS-198.

References

[1] D. A. Ehst, S. Kim, Y. Gohar, L. Turner, D. L. Smith, and R. Mattas, "Application of high temperature ceramic superconductors (CSC) to commercial tokamak reactors," *Fusion Technology*, vol. 15, no. 2, pp. 1021–1031, 1989.

[2] L. Bromberg, M. Tekula, L. A. El-Guebaly, and R. Miller, "Options for the use of high temperature superconductor in tokamak fusion reactor designs," *Fusion Engineering and Design*, vol. 54, no. 2, pp. 167–180, 2001.

[3] K. Okuno, A. Shikov, and N. Koizumi, "Superconducting magnet system in a fusion reactor," *Journal of Nuclear Materials*, vol. 329-333, no. 1-3, pp. 141–147, 2004.

[4] S. I. Schlachter, W. Goldacker, F. Grilli, R. Heller, and A. Kudymow, "Coated conductor rutherford cables (CCRC) for high-current applications: Concept and properties," *IEEE Transactions on Applied Superconductivity*, vol. 21, no. 3, pp. 3021–3024, 2011.

[5] D. C. Van Der Laan, P. D. Noyes, G. E. Miller, H. W. Weijers, and G. P. Willering, "Characterization of a high-temperature superconducting conductor on round core cables in magnetic fields up to 20 T," *Superconductor Science and Technology*, vol. 26, no. 4, Article ID 045005, 2013.

[6] G. Celentano, G. De Marzi, F. Fabbri et al., "Design of an industrially feasible twisted-stack HTS cable-in-conduit conductor for fusion application," *IEEE Transactions on Applied Superconductivity*, vol. 24, no. 3, 2014.

[7] S. Hahn, J. Song, Y. Kim et al., "Design study on a 100-kA/20-K HTS cable for fusion magnets," *IEEE Transactions on Applied Superconductivity*, vol. 25, no. 3, 2015.

[8] D. Uglietti, N. Bykovsky, and K. Sedlak, "Test of 60 kA coated conductor cable prototypes for fusion magnets," *Superconductor Science & Technology*, vol. 28, no. 12, Article ID 124005, 2015.

[9] T. Ando, T. Isono, K. Hamada et al., "Design of a 60-kA HTS Current Lead for Fusion Magnets and its RD," *IEEE Trans. on Applied Superconductivity*, vol. 11, no. 1, pp. 2535–2538, 2001.

[10] R. Heller, S. M. Darweschsad, G. Dittrich et al., "Experimental results of a 70 kA high temperature superconductor current lead demonstrator for the ITER magnet system," *IEEE Transactions on Applied Superconductivity*, vol. 15, no. 2, pp. 1496–1499, 2005.

[11] J. H. Schultz, G. Driscoll, D. Gamier et al., "High temperature superconducting levitation coil for the Levitated Dipole Experiment (LDX)," *IEEE Transactions on Applied Superconductivity*, vol. 11, no. 1, pp. 2004–2009, 2001.

[12] S. Tanaka and H. Takatsu, "Japanese perspective of fusion nuclear technology from ITER to DEMO," *Fusion Engineering and Design*, vol. 83, no. 7-9, pp. 865–869, 2008.

[13] Z. S. Hartwig, C. B. Haakonsen, R. T. Mumgaard, and L. Bromberg, "An initial study of demountable high-temperature superconducting toroidal field magnets for the Vulcan tokamak conceptual design," *Fusion Engineering and Design*, vol. 87, no. 3, pp. 201–214, 2012.

[14] T. Ando, T. Kato, K. Ushigusa et al., "Design of the toroidal field coil for A-SSTR2 using high Tc superconductor," *Fusion Engineering and Design*, vol. 58-59, pp. 13–16, 2001.

[15] T. Ando and S. Nishio, "Design of the TF Coil for a Tokamak Fusion Power Reactor with YBCO Tape Superconductors," in *Proceedings of the 21st IEEE/NPS Symposium on Fusion Engineering SOFE 05*, pp. 1–4, Knoxville, TN, USA, September 2005.

[16] Y. Zhang, Y. Tang, C. Zhang, Z. Xia, and L. Ren, "Performance and Analysis of No-Insulation HTS Toroidal Magnet," *IEEE*

Transactions on Applied Superconductivity, vol. 27, no. 4, pp. 1–5, 2017.

[17] S. B. Kim, T. Kaneko, H. Kajikawa et al., "The transient stability of HTS coils with and without the insulation and with the insulation being replaced by brass tape," *IEEE Transactions on Applied Superconductivity*, vol. 23, no. 3, 2013.

[18] T. Wang, S. Noguchi, X. Wang et al., "Analyses of transient behaviors of no-insulation REBCO pancake coils during sudden discharging and overcurrent," *IEEE Transactions on Applied Superconductivity*, vol. 25, no. 3, 2015.

[19] Y. Wang, H. Song, and D. Xu, *An equivalent circuit grid model for no-insulation HTS pancake coils*, Superconductor Science & Technology, Superconductor Science, 2015.

[20] X. Wang, S. Hahn, Y. Kim et al., "Turn-to-turn contact characteristics for an equivalent circuit model of no-insulation ReBCO pancake coil," *Superconductor Science and Technology*, vol. 26, no. 3, Article ID 035012, 2013.

[21] Y. Xu, Y. Tang, L. Ren et al., "Distribution of AC loss in a HTS magnet for SMES with different operating conditions," *Physica C: Superconductivity and its Applications*, vol. 494, pp. 213–216, 2013.

[22] H. Fujishiro, T. Naito, and D. Furuta, "Analysis of temperature and magnetic field distribution in superconducting bulk during pulsed field magnetization," *IEEE Transactions on Applied Superconductivity*, vol. 21, no. 3, pp. 2723–2726, 2011.

[23] R. Siegal and J. R. Howell, *Thermal Radiation Heat Transfer*, Hemisphere, Bristol, PA, USA, 2nd edition, 1981.

[24] American Cryomech Company Co. Ltd., http://www.cryomech.com/products/cryorefrigerators/gifford/al325/.

[25] CSIC Pride (Nanjing) Cryogenic Technology Co, http://www.724pridecryogenics.com/upload/edit_tool/061211300.pdf.

[26] J. Li, Q. Wang et al., "Analysis of Temperature Rise of TF Magnet During Plasma Discharges on EAST," *IEEE Transactions on Applied Superconductivity*, vol. 24, no. 3, Article ID 4203005, 2014.